

## Threshold-Based TOA Estimation for Impulse Radio UWB Systems

I. Guvenc and Z. Sahinoglu

TR2005-026 December 2005

### Abstract

Highly dispersive nature of ultra-wideband (UWB) channels makes time of arrival (TOA) estimation extremely challenging, where the leading-edge path is not necessarily the strongest path. Since the bandwidth of a received UWB signal is very large, the Nyquist rate sampling becomes impractical, hence motivating lower complexity and yet accurate ranging techniques at feasible sampling rates. In this paper, we consider TOA estimation based on symbol rate samples that are obtained after a square-law device. An adaptive threshold selection approach based on the minimum and maximum values of the energy samples is introduced, and optimal values of the thresholds for different signal to noise ratios (SNRs) are investigated via simulations. Theoretical closed form expressions are derived for mean absolute TOA estimation error, and compared with simulations using IEEE 802.15.4a channel models.

*IEEE ICU*

This work may not be copied or reproduced in whole or in part for any commercial purpose. Permission to copy in whole or in part without payment of fee is granted for nonprofit educational and research purposes provided that all such whole or partial copies include the following: a notice that such copying is by permission of Mitsubishi Electric Research Laboratories, Inc.; an acknowledgment of the authors and individual contributions to the work; and all applicable portions of the copyright notice. Copying, reproduction, or republishing for any other purpose shall require a license with payment of fee to Mitsubishi Electric Research Laboratories, Inc. All rights reserved.



# Threshold-Based TOA Estimation for Impulse Radio UWB Systems

I. Guvenc<sup>1,2</sup>, Z. Sahinoglu<sup>1</sup>

<sup>1</sup>Mitsubishi Electric Research Labs, 201 Broadway Ave., Cambridge, MA, 02139

<sup>2</sup>Department of Electrical Engineering, University of South Florida, Tampa, FL, 33620  
E-mail: {guvenc, zafer}@merl.com

**Abstract**—Highly dispersive nature of ultra-wideband (UWB) channels makes time of arrival (TOA) estimation extremely challenging, where the leading-edge path is not necessarily the strongest path. Since the bandwidth of a received UWB signal is very large, the Nyquist rate sampling becomes impractical, hence motivating lower complexity and yet accurate ranging techniques at feasible sampling rates. In this paper, we consider TOA estimation based on symbol rate samples that are obtained after a square-law device. An adaptive threshold selection approach based on the minimum and maximum values of the energy samples is introduced, and optimal values of the thresholds for different signal to noise ratios (SNRs) are investigated via simulations. Theoretical closed form expressions are derived for mean absolute TOA estimation error, and compared with simulations using IEEE 802.15.4a channel models.

## I. INTRODUCTION

High time resolution is one of the key benefits of ultra-wideband (UWB) signals for precision ranging. Due to extremely short duration of transmitted UWB pulses, UWB receivers, as opposed to typical narrow-band wireless receivers, enjoy being able to observe individual multipath components; and the accuracy of TOA estimation is characterized by how finely the first arriving signal path is identified, which may not be the strongest.

UWB receivers typically have to operate at very low sampling rates. This makes it difficult to effectively capture the energy at each individual multipath component using Rake receivers, as it is extremely difficult to synchronize to each tap. A chip-spaced sampling of the channel can be used to detect the chip-spaced *observation* of the channel impulse response (CIR), which typically carries a fraction of the available energy of the actual CIR. Note that higher rate samples (such as chip-rate or frame-rate) can be achieved by using symbol-spaced sampling and multiple training symbols, and shifting the signal by desired sampling period at each symbol. Another practical concern is the requirement to have a-priori knowledge of the received pulse shape for match filter implementation, which may change from an environment to another and even between different multipath components [1]. Therefore, it is difficult to exactly match to the received pulse-shape, especially when considering the analog implementations of the template waveforms.

Typical approaches for UWB ranging in the literature are based on matched filtering (MF) of the received signal. Corresponding the time index that maximizes the MF output to the TOA estimate is probably the simplest ranging technique [2]-[6]. These approaches have limited TOA precision, as the strongest path is not necessarily the first arriving path. In order to determine the leading edge of a received signal, Lee and Scholtz proposed to use a generalized maximum-likelihood (GML) approach to search the paths prior to the

strongest path [7]; however, the information included in the paths after the strongest path were neglected, which can be used to enhance strongest path detection. In [8], the leading edge detection problem is taken as a break-point estimation of the actual signal itself, where temporal correlation arising from the transmitted pulse is used to accurately partition the received signal into two zero-mean Gaussian distributed time-series with different covariance matrices. In both [7], [8], very high sampling rates were considered, which is not practical in many scenarios; a threshold-based technique with lower-rate samples was discussed in [9]. In another lower sampling-rate approach, a two-step ranging algorithm is considered, where an energy detection step gives coarse information about the signal's whereabouts, and a correlation based approach is applied into the detected energy block(s) for refinement [10].

Due to above practical concerns and limitations, energy detection based ranging becomes more feasible. Even though it suffers more from noise due to a square-law device, energy detection does not require accurate timing or pulse shapes. Once collecting the energy samples at the output of a square-law device, the TOA estimation can be considered as a problem of leading edge detection (or change/break-point detection) in noise. In this paper, we consider TOA estimation of the received signal based on symbol-rate samples, and analyze via theory and simulations the performance of threshold based leading edge detection techniques. A simple normalized threshold comparison (TC) approach is proposed, where only the minimum and maximum energy values are used. Dependence of the optimum threshold and mean absolute error (MAE) on signal to noise ratio (SNR) and channel model are investigated. Theoretical expressions for MAE are derived for the fixed threshold case, and compared with simulations. Also, maximum energy selection (MES) algorithm, as well as MES supported with search-back step (MES-SB) are analyzed, and dependence of optimal search-back window to the SNR is demonstrated. Simulation results reveal the performance trade-off's of the algorithms for different channel models and block sizes.

## II. SYSTEM MODEL

Let the received UWB multipath signal be represented as

$$r(t) = \sum_{j=-\infty}^{\infty} d_j \omega_{mp}(t - jT_f - c_j T_c - \tau_{toa}) + n(t) \quad (1)$$

where frame index and frame duration are denoted by  $j$  and  $T_f$ ,  $N_s$  represents the number of pulses per symbol,  $T_c$  is the chip duration,  $T_s$  is the symbol duration,  $\tau_{toa}$  is the TOA of the received signal, and  $N_h$  is the possible number of chip positions per frame, given by  $N_h = T_f/T_c$ . Effective pulse

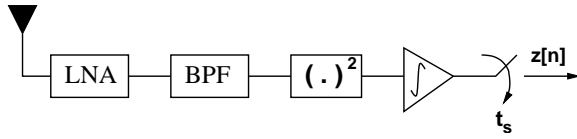


Fig. 1. Sampling of the received signal after energy detection.

after the channel impulse response is given by  $\omega_{mp}(t) = \sqrt{E} \sum_{l=1}^L \alpha_l \omega(t - \tau_l)$ , where  $\omega(t)$  is the received UWB pulse with unit energy,  $E$  is the pulse energy,  $\alpha_l$  and  $\tau_l$  are the fading coefficients and delays of the multipath components, respectively. Additive white Gaussian noise (AWGN) with zero-mean and double-sided power spectral density  $\mathcal{N}_0/2$  and variance  $\sigma^2$  is denoted by  $n(t)$ . No modulation is considered for the ranging process.

In order to avoid catastrophic collisions, and smooth the power spectral density of the transmitted signal, time-hopping codes  $c_j^{(k)} \in \{0, 1, \dots, N_h - 1\}$  are assigned to different users. Moreover, random-polarity codes  $d_j \in \{\pm 1\}$  are used to introduce additional processing gain for the detection of desired signal, and smooth the signal spectrum.

#### A. Sampling of the Received Signal After a Square-law Device

In the sequel, we assume that a coarse acquisition on the order of frame-length is acquired in (1), such  $\tau_{toa} \sim \mathcal{U}(0, T_f)$ , where  $\mathcal{U}(\cdot)$  denotes the uniform distribution. As for the search region, the signal within time frame  $T_f$  plus half of the next frame is considered to factor-in inter-frame leakage due to multipath, and the signal is then input to a bank of square-law devices each with an integration interval of  $T_b$  (see Fig. 1).

The number of samples (or blocks) is denoted by  $N_b = \frac{3}{2} \frac{T_f}{T_b}$ , and  $n \in \{1, 2, \dots, N_b\}$  denotes the sample index with respect to the starting point of the uncertainty region. With a sampling interval of  $t_s$  (which is equal to block length  $T_b$ ), the sample values at the output of the square-law device are given by

$$z[n] = \sum_{j=1}^{N_s} \int_{(j-1)T_f + (c_j + n-1)T_b}^{(j-1)T_f + (c_j + n)T_b} |r(t)|^2 dt, \quad (2)$$

and the performance can be further improved by using the energy in  $N_T$  symbols. The bit energy when using  $N_s$  pulses becomes  $E_b = N_s E$ . Basic TOA estimation algorithms that operate on  $z[n]$  values for leading edge detection will be presented and formulated in the next section.

### III. TOA ESTIMATION ALGORITHMS

Choosing the maximum energy output to be the leading edge is the simplistic way of achieving a TOA estimation. Using MES, the TOA estimate with respect to the beginning of the time frame is evaluated as  $\hat{t}_{MES} = \left[ \operatorname{argmax}_{1 \leq n \leq N_b} \{z[n]\} - 0.5 \right] T_b = (n_{max} - 0.5) T_b$ , where the center of the block is selected as the TOA estimate. Note that on the average, selecting the center of the block gives a resolution of quarter of the block size. However, the strongest energy block in many cases may not be the leading energy block (Fig. 3), and the MES therefore hits an error-floor even in high signal to noise ratio (SNR) region. Also, the performance of it degrades with

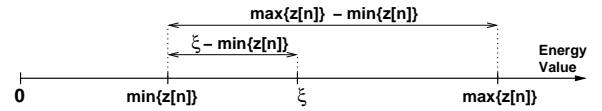


Fig. 2. Illustration of the normalized adaptive threshold depending on the minimum and maximum energy samples.

$N_b$ , since it becomes more likely to identify a noise only block as the maximum energy block [11].

Received samples can be also compared to an appropriate threshold, and the first threshold-exceeding sample index can be corresponded as the TOA estimate, i.e.  $t_{TC} = \left[ \min\{n | z[n] > \xi\} - 0.5 \right] T_b$ , where  $\xi$  is a threshold that must be set based on the received signal statistics. Given the minimum and maximum energy sample values, the following normalized adaptive threshold can be used (see Fig. 2)

$$\xi_{norm} = \frac{\xi - \min\{z[n]\}}{\max\{z[n]\} - \min\{z[n]\}}. \quad (3)$$

Optimal value of  $\xi_{norm}$  (i.e.,  $\xi_{opt}$ ) changes depending on the SNR as discussed later in the paper.

In order to improve the performance of the TC in low SNRs, the energy samples prior to the maximum should be searched. The TOA estimate with a thresholding and backward search is then given by  $\hat{t}_{MES-SB} = \left[ \min\{n | \tilde{z}[n] < \xi\} - 0.5 + (n_{max} - w_{sb} - 1) \right] T_b$ , where  $\tilde{z}[n] = \left[ z[n_{max} - w_{sb}], z[n_{max} - w_{sb} + 1] \dots z[n_{max}] \right]$ . Search-back window in number of samples is denoted by  $w_{sb}$ , which is set based on the statistics of the channel, and is  $\lceil W_{sb} N_s / T_b \rceil$  with  $W_{sb}$  denoting the window size in time units. Note that the accuracy of this approach is also limited by the accuracy of the MES. The basic TOA estimation algorithms are summarized in Fig. 3.

### IV. ERROR ANALYSIS FOR TC BASED TOA ESTIMATION

In this section, mean absolute error (MAE) of the TC based TOA estimation is analyzed, and closed form error expressions are presented. First, the probability of detection of a certain block is derived, which leads us to the derivation of MAE of the TOA estimate for the case of uniformly distributed TOA. Assume initially that the delay of the leading-edge energy block is fixed. Let  $n_{toa}$  denote the first arriving energy block index,  $\hat{n}$  denote the estimated block index, and  $n = 1, 2, \dots, N_B$  denote the block indices where the energy block is being searched. Then, fixing the value of threshold  $\xi$ , probability of detecting an arbitrary block  $n_{hyp}$  to be the energy block is calculated as<sup>1</sup>

$$\begin{aligned} P_D(n_{hyp}) &= P(\hat{n} = n_{hyp}) \\ &= \left[ \prod_{n=1}^{n_{hyp}-1} P(z[n] < \xi) \right] \times P(z[n_{hyp}] > \xi), \end{aligned} \quad (4)$$

where  $z[n]$  has a centralized Chi-square distribution for  $n = 1, 2, \dots, n_{toa} - 1$  (corresponding to noise-only blocks), and non-centralized Chi-square distribution for  $n = n_{toa}$ . The

<sup>1</sup>Note that this is valid for  $n_{hyp} \geq 2$ . For  $n_{hyp} = 1$ , the terms corresponding to noise blocks become unity.

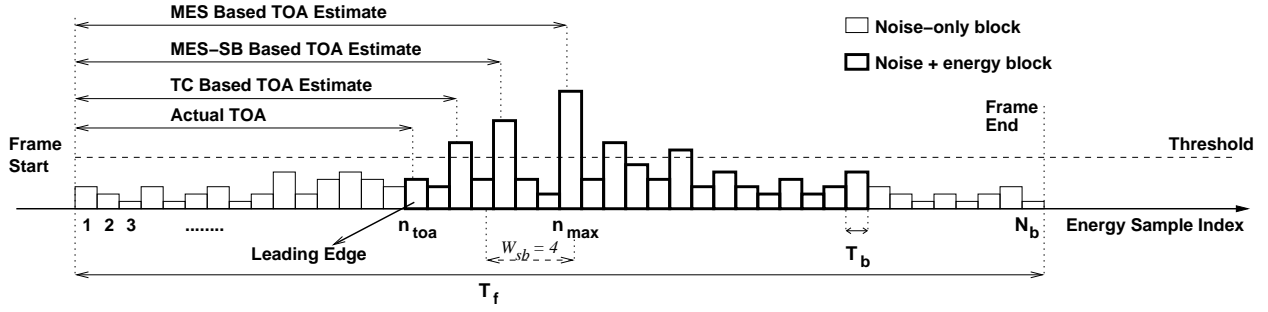


Fig. 3. Illustration of basic TOA estimation techniques based on energy samples.

cumulative distribution functions (CDFs) of these centralized and non-centralized Chi-square random variables are given by

$$P_{chi2}(\xi) = P(z[n] < \xi) = 1 - \exp\left(-\frac{\xi}{2\sigma^2}\right) \sum_{l=0}^{M/2-1} \frac{1}{l!} \left(\frac{\xi}{2\sigma^2}\right)^l, \quad (5)$$

$$P_{ncx2}(E_n, \xi) = P(z[n] < \xi) = 1 - Q_{M/2}\left(\frac{E_n}{\sigma}, \sqrt{\frac{\xi}{\sigma}}\right), \quad (6)$$

where  $\sigma^2 = \frac{N_0}{2}$  is the noise variance,  $Q_x(\cdot)$  denotes the Marcum-Q function with parameter  $x$ , and  $E_n$  is the signal energy within the  $n$ th block, whose PDF varies with  $n$ , block size, and channel model. Note that  $n_{hyp} = n_{toa}$  corresponds to correct detection. Fixing the value of  $\xi$ , three cases can be considered for  $n_{hyp}$ . If  $n_{hyp} < n_{toa}$ , we have

$$P_D(n_{hyp}) = [P_{chi2}(\xi)]^{n_{hyp}-1} (1 - P_{chi2}(\xi)), \quad (7)$$

while on the other hand if  $n_{hyp} = n_{toa}$ ,

$$P_D(n_{hyp}) = [P_{chi2}(\xi)]^{n_{toa}-1} \times \int_{E_{n_{toa}}} \left(1 - P_{ncx2}(E_{n_{toa}}, \xi)\right) p(E_{n_{toa}}) dE_{n_{toa}}. \quad (8)$$

If  $n_{hyp} > n_{toa}$ , we can further consider two conditions. Let  $N_{eb}$  denote the number of noise plus energy blocks where there exists a significant amount of energy. If  $n_{hyp} - n_{toa} < N_{eb}$

$$P_D(n_{hyp}) = [P_{chi2}(\xi)]^{n_{toa}-1} \times \left( \prod_{n=n_{toa}}^{n_{hyp}-1} \int_{E_n} P_{ncx2}(E_n, \xi) p(E_n) dE_n \right) \times \int_{E_{n_{hyp}}} \left(1 - P_{ncx2}(E_{n_{hyp}}, \xi)\right) p(E_{n_{hyp}}) dE_{n_{hyp}}, \quad (9)$$

while, if  $n_{hyp} - n_{toa} \geq N_{eb}$

$$P_D(n_{hyp}) = [P_{chi2}(\xi)]^{n_{hyp}-N_{eb}-1} \left(1 - P_{chi2}(\xi)\right) \times \prod_{n=n_{toa}}^{n_{toa}+N_{eb}-1} \int_{E_n} P_{ncx2}(E_n, \xi) p(E_n) dE_n. \quad (10)$$

In order to carry out the evaluation of the detection probabilities, the energy PDFs  $p(E_n)$  are obtained via simulations

(see Fig. 6) with considering the uniformly distributed delay offsets of the individual paths within the blocks. Note that in order to calculate closed form expressions for the detection probabilities in the case of normalized thresholds presented in (3) rather than fixed thresholds, the PDFs of  $\xi_{norm}$  can be used. However, our simulations show that especially for large  $E_b/N_0$  values,  $\xi_{norm}$  is highly correlated with the energies in the first couple of energy blocks, with correlation coefficients being on the order of 0.6 at  $E_b/N_0 = 26dB$  for the first four energy plus noise blocks. This implies that the PDFs of  $\xi_{norm}$  also has to be conditioned on  $E_n$ , which makes closed form error analysis cumbersome and analytically intractable for variable  $\xi$ .

Given  $n_{toa}$  to be fixed, the MAE can be calculated by averaging over the probability of detection of different TOA estimations:

$$e_{abs}[n_{toa}] = E[|\hat{n} - n|] = \sum_{n=1}^{N_b} P_D(n) \times |n - n_{toa}|. \quad (11)$$

In other words, the absolute error corresponding to each block are weighted by the probability of detecting that particular block. For  $n_{toa} \sim \mathcal{U}(1, N_B)$ , we can average  $e_{abs}[n_{toa}]$  to obtain the average error as

$$e_{abs}^{(avg)} = \sum_{n_{toa}=1}^{N_b} e_{abs}[n_{toa}] p(n_{toa}) = \frac{1}{N_b} \sum_{n_{toa}=1}^{N_b} e_{abs}[n_{toa}]. \quad (12)$$

## V. RESULTS AND DISCUSSION

In all the simulations that are presented in this section, the channel models CM1 (residential LOS) and CM2 (residential NLOS) of IEEE802.15.4a are employed. The channel realizations are sampled at 8GHz, 1000 different realizations are generated, and each realization has a TOA uniformly distributed within  $(0, T_f)$ . A raised cosine pulse of  $T_c = 1ns$  is considered for all scenarios. After introducing uniformly distributed delays, energies are collected within non-overlapping windows to obtain decision statistics. Two critical statistics for the accuracy of the TOA estimation at this step are the PDF of the energy of the maximum energy block (Fig. 4), and the PDF of the delay between the maximum energy block and the leading edge block (Fig. 5), where distinctions between LOS CM1 and NLOS CM2 channel models can be clearly observed. Also in Fig. 6, PDFs of the energies within the first four blocks including and after the leading edge block are presented. These PDFs are used to evaluate the theoretical expressions derived in previous section. The other simulation

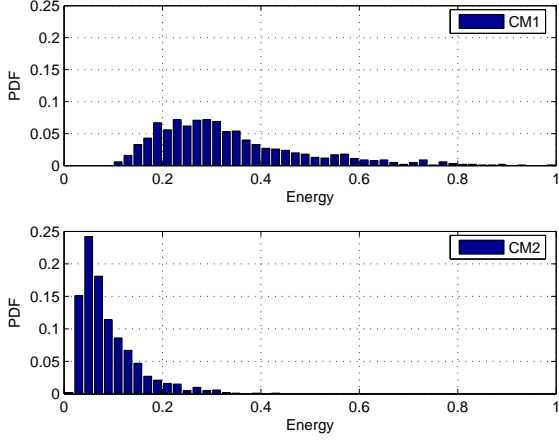


Fig. 4. Comparison of the PDFs of energy of maximum energy block for CM1 and CM2 ( $T_b = 1\text{ns}$ ).

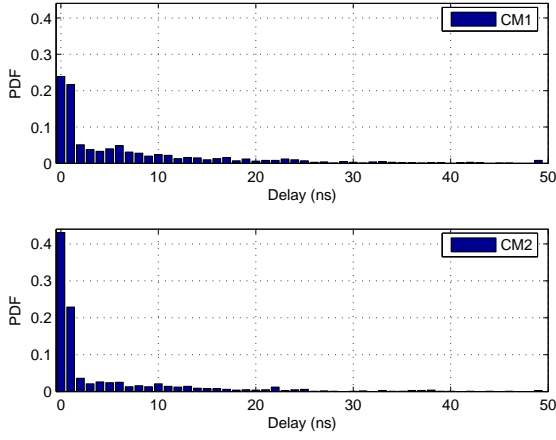


Fig. 5. Comparison of the PDFs of the arrival time of maximum energy block with respect to the first energy block for CM1 and CM2 ( $T_b = 1\text{ns}$ ).

parameters are (unless otherwise stated)  $T_f = 200\text{ns}$ ,  $B = 4\text{GHz}$ ,  $N_T = 1$ , and  $N_s = 1$ . Both  $1\text{ns}$  and  $4\text{ns}$  are considered for  $T_b$ .

#### A. Normalized Threshold Characteristics of CM1 and CM2

TOA estimation errors with respect to the employed normalized threshold for various  $E_b/N_0$  are given in Fig. 7 for CM1 and in Fig. 8 for CM2. If SNR estimate is available, the value  $\xi_{norm}$  that minimizes the MAE can be selected. On the other hand, it is observed that selecting  $\xi_{norm}$  to be on the order of 0.8 will yield near optimal performance at almost every  $E_b/N_0$  under CM2, while for CM1 it must be closer to 0.2 at high  $E_b/N_0$ , but may be selected as 0.4 to cover a larger range of SNR values. Regardless of the threshold selection, at  $E_b/N_0 < 20\text{dB}$  the MAE becomes intolerably high for sub-meter resolution ranging. The optimal threshold levels with respect to  $E_b/N_0$  for CM1 and CM2, as well as the corresponding minimum MAE values are depicted in Fig 9, 10 for better visualization.

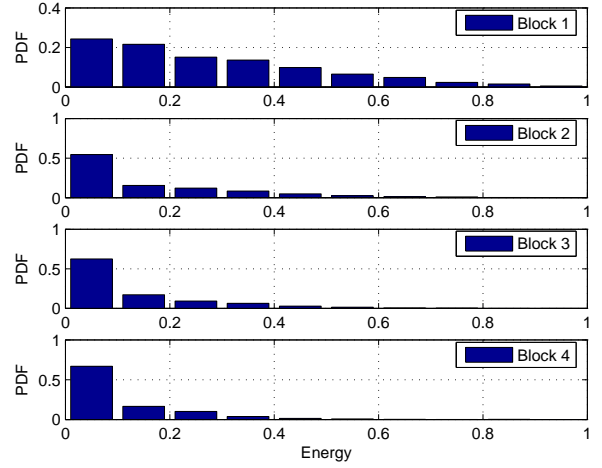


Fig. 6. PDFs of block energies in the first four energy blocks ( $T_b = 4\text{ns}$ ). Uniformly distributed delay of the first arriving path within the block interval is considered.

#### B. Comparison of TC Based TOA Estimation Using Theory and Simulations

The theoretical and simulated performances of threshold based TOA estimators when using a fixed threshold of  $0.1 \times E_b$  at all  $E_b/N_0$  are given in Fig. 11 for CM1 ( $T_b = 4\text{ns}$ ). The PDFs obtained via simulations in Fig. 6 are used to average the performances over the energy distributions. The PDFs of the first 8 blocks including and after  $n_{toa}$  are included only, considering the rest of the blocks to be noise-only blocks. Even though the error expression in (12) shows a good match with simulation at low  $E_b/N_0$  (where the ranging error is unacceptably bad), it yields optimistic results compared to simulations at large  $E_b/N_0$ .

The performance of the threshold based TOA estimation can be improved using an adaptive threshold, as discussed in previous sections. Given  $\max\{z[n]\}$  and  $\min\{z[n]\}$ , optimum adaptive normalized threshold values that corresponds to the operated  $E_b/N_0$  can be used to have a superior performance compared to a fixed threshold (excluding very high SNRs). However, this requires estimation of the SNR, which is not an easy task in UWB due to extremely low power operation characteristics. Instead, an adaptive normalized threshold  $\xi_{norm}$  can be used at all SNR values. As an example,  $\xi_{norm} = 0.5$  is used in Fig. 11, which shows to match with the optimum threshold results at  $E_b/N_0 = 22\text{dB}$ , and performs suboptimal otherwise.

As a final remark, at  $E_b/N_0 = 26\text{dB}$ , it is observed that a fixed threshold performs better than the optimal adaptive threshold. This is due to the fact that optimal threshold values obtained via simulations are optimal *given* the knowledge of only  $\max\{z[n]\}$  and  $\min\{z[n]\}$ . The fixed threshold values used for demonstrating theoretical and simulation results in Fig. 11 assumes the knowledge of the received energy value, which is not exploited in the adaptive threshold estimation.

#### C. Dependence of Optimal Search-back Window on the SNR

In Fig. 12, the MAE performances with respect to  $W_{sb}$  are investigated with  $\xi_{norm}$  fixed to 0.4 and 0.8 for CM1 and CM2, respectively. It is observed that for CM1, a search-back

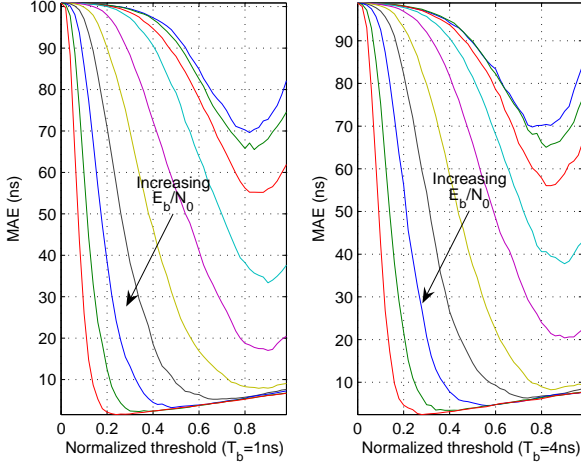


Fig. 7. MAE of TOA estimation under CM1 with respect to the normalized threshold for  $E_b/N_0 = \{8, 10, 12, 14, 16, 18, 20, 22, 24, 26\}$ dB.

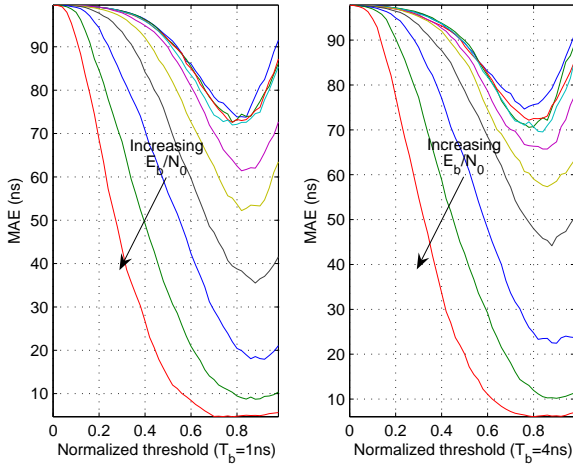


Fig. 8. MAE of TOA estimation under CM2 with respect to the normalized threshold for  $E_b/N_0 = \{8, 10, 12, 14, 16, 18, 20, 22, 24, 26\}$ dB.

window on the order of 30ns will yield satisfactory results for a large range of SNR values. On the other hand, even though dependency of the MAE to  $W_{sb}$  is weaker, fixing it to 40ns will yield slight improvements in the estimation accuracy.

#### D. Comparison of Performances of Various TOA Estimation Algorithms

In Figs. 13-14, the performances of different energy detection based TOA estimation algorithms are tested in IEEE 802.15.4a CM1 and CM2. The  $\xi_{opt}$  is set to 0.4 for CM1 and to 0.8 for CM2, with the assumption that there is no SNR estimate available. Also, corresponding  $W_{sb}$  are set to 30ns and 40ns for CM1 and CM2, respectively (as evaluated in the previous sections). It is observed that the TC performs well at high  $E_b/N_0$ , while the MES is better at higher noise variance. The reason for TC performing poorly in general at low SNR region is frequent threshold exceeding caused by noise. On the other hand, when the SNR is large, the TC does not face an early error floor as opposed to the MES. Using a block of 1ns rather than 4ns yields on the order of a nanosecond

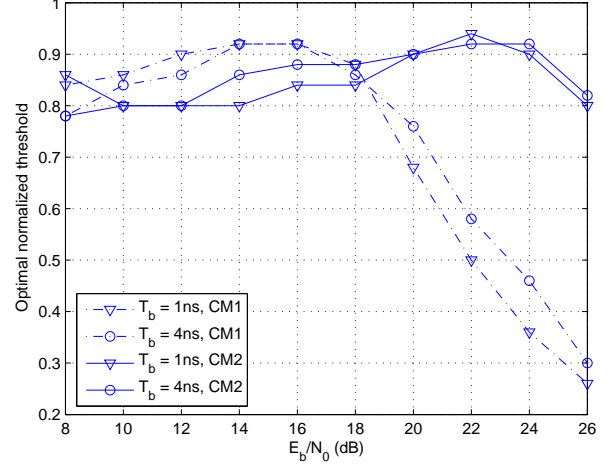


Fig. 9. Optimum normalized thresholds with respect to  $E_b/N_0$  under CM1 and CM2, and for  $T_b = 1$ ns and  $T_b = 4$ ns.

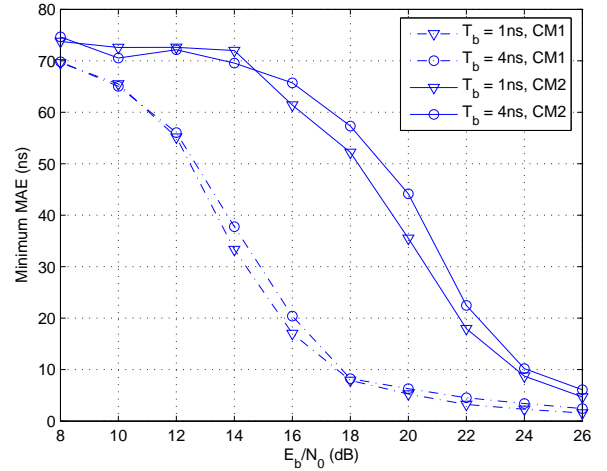


Fig. 10. Minimum MAEs with respect to  $E_b/N_0$  under CM1 and CM2, and for  $T_b = 1$ ns and  $T_b = 4$ ns.

improvement in the accuracy for the large SNR region, which can be explained by previous discussion that the average TOA estimation accuracy is on the order of quarter the block length.

The performance difference under CM1 and CM2 is on the order of 3dB to 6dB in favor of CM1 for low to moderate SNR ranges. This can be explained by Fig. 4, where the probability of large energy values is shown to be much larger for CM1 compared to CM2. On the other hand, once the TOA estimation errors hit the error floor, algorithms perform slightly better under CM2 than CM1. The explanation for this phenomena comes with Fig. 5, where it is indicated that even though the energy values are small, they are more frequently closer to the leading edge for CM2.

## VI. CONCLUSION

Various TOA estimation algorithms for low sampling rate UWB systems based on energy detection are analyzed. An adaptive threshold selection approach that makes use of the minimum and maximum energy samples is introduced, and optimum threshold values are demonstrated via simulations for

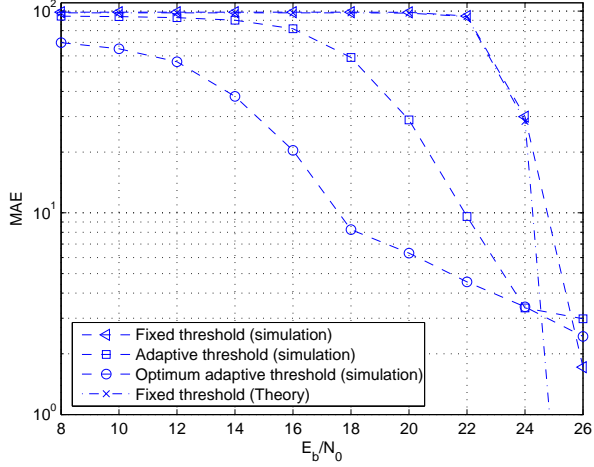


Fig. 11. Comparison of theoretical and simulation results with respect to  $E_b/N_0$  for fixed and adaptive threshold based TOA estimation algorithms (CM1,  $T_b = 4\text{ns}$ ).

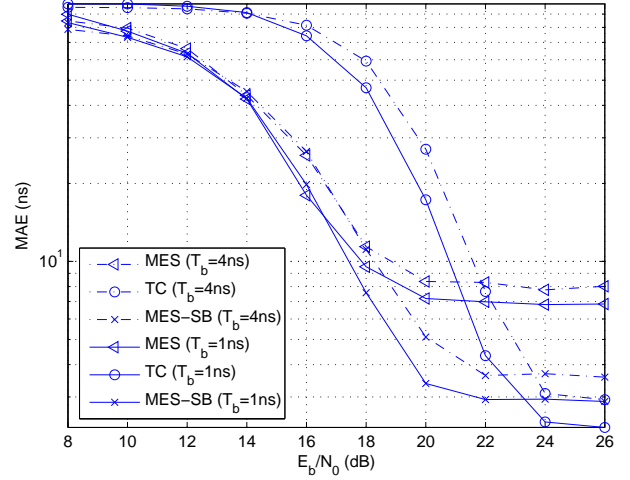


Fig. 13. Absolute error plots for different algorithms with respect to  $E_b/N_0$  (CM1,  $\xi_{norm} = 0.4$ ,  $W_{sb} = 30\text{ns}$ ).

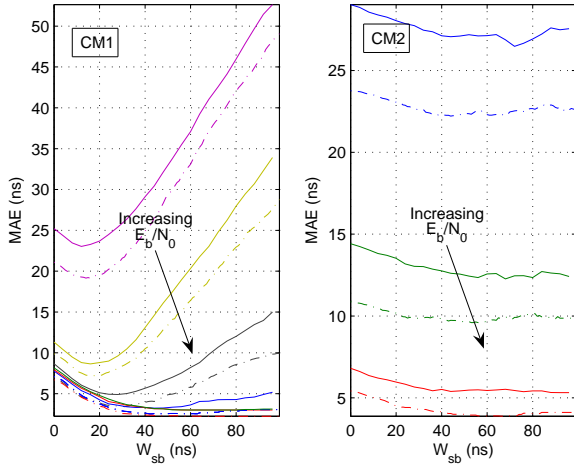


Fig. 12. MAE of TOA estimation with respect to search-back window size under CM1 ( $E_b/N_0 = \{16, 18, 20, 22, 24, 26\}\text{dB}$ ,  $\xi_{norm} = 0.4$ ) and CM2 ( $E_b/N_0 = \{22, 24, 26\}\text{dB}$ ,  $\xi_{norm} = 0.8$ ), for block sizes of 1ns (dashed) and 4ns (solid).

CM1 and CM2 channels. Closed form expressions for MAE for the fixed threshold case are derived and compared with simulations, yielding good match at low to moderate  $E_b/N_0$  ranges. Simulations show that the maximum energy selection supported with a search-back step performs better than other algorithms except the TC algorithm at very high SNR.

## REFERENCES

- [1] R. Qiu, "A study of the ultra-wideband wireless propagation channel and optimum UWB receiver design," *IEEE J. Select. Areas Commun.*, vol. 20, no. 9, pp. 1628–1637, Dec. 2002.
- [2] W. Chung and D. Ha, "An accurate ultra wideband (UWB) ranging for precision asset location," in *Proc. IEEE Conf. Ultrawideband Syst. Technol. (UWBST)*, Reston, VA, Nov. 2003, pp. 389–393.
- [3] B. Denis, J. Keignart, and N. Daniele, "Impact of NLOS propagation upon ranging precision in UWB systems," in *Proc. IEEE Conf. Ultrawideband Syst. Technol. (UWBST)*, Reston, VA, Nov. 2003, pp. 379–383.
- [4] K. Yu and I. Oppermann, "Performance of UWB position estimation based on time-of-arrival measurements," in *Proc. IEEE Conf. Ultrawideband Syst. Technol. (UWBST)*, Kyoto, Japan, May 2004, pp. 400–404.

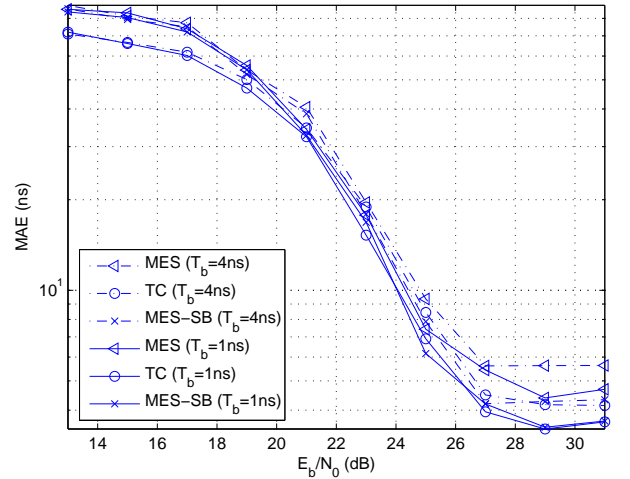


Fig. 14. Absolute error plots for different algorithms with respect to  $E_b/N_0$  (CM2,  $\xi_{norm} = 0.8$ ,  $W_{sb} = 40\text{ns}$ ).

- [5] A. Rabbachin and I. Oppermann, "Synchronization analysis for UWB systems with a low-complexity energy collection receiver," in *Proc. IEEE Conf. Ultrawideband Syst. Technol. (UWBST)*, Kyoto, Japan, May 2004, pp. 288–292.
- [6] R. Fleming, C. Kushner, G. Roberts, and U. Nandiwada, "Rapid acquisition for ultra-wideband localizers," in *Proc. IEEE Conf. Ultrawideband Syst. Technol. (UWBST)*, Baltimore, MD, May 2002, pp. 245–249.
- [7] J.-Y. Lee and R. A. Scholtz, "Ranging in a dense multipath environment using an UWB radio link," *IEEE J. Select. Areas Commun.*, vol. 20, no. 9, pp. 1677–1683, Dec. 2002.
- [8] C. Mazzucco, U. Spagnolini, and G. Mulas, "A ranging technique for UWB indoor channel based on power delay profile analysis," in *Proc. IEEE Vehic. Technol. Conf. (VTC)*, Los Angeles, CA, Sep. 2004, pp. 2595–2599.
- [9] R. A. Scholtz and J. Y. Lee, "Problems in modeling UWB channels," in *Proc. IEEE Asilomar Conf. Signals, Syst. Computers*, vol. 1, Monterey, CA, Nov. 2002, pp. 706–711.
- [10] S. Gezici, Z. Sahinoglu, H. Kobayashi, and H. V. Poor, *Ultra Wideband Geolocation*. John Wiley & Sons, Inc., 2005, in Ultrawideband Wireless Communications.
- [11] I. Guvenc and Z. Sahinoglu, "Low complexity TOA estimation for impulse radio UWB systems using multiscale energy products," in *Submitted to IEEE Global Telecommun. Conf. (GLOBECOM)*, St. Louis, MO, Dec. 2005.